



HAL
open science

Free-standing cellulose film containing manganese dioxide nanoparticles and its use in discoloration of indigo carmine dye

Larissa V.F. Oliveira, Simona Bennici, Ludovic Josien, Lionel Limousy,
Marcos Bizeto, Fernanda Camilo

► To cite this version:

Larissa V.F. Oliveira, Simona Bennici, Ludovic Josien, Lionel Limousy, Marcos Bizeto, et al.. Free-standing cellulose film containing manganese dioxide nanoparticles and its use in discoloration of indigo carmine dye. *Carbohydrate Polymers*, 2019, pp.115621. 10.1016/j.carbpol.2019.115621 . hal-02382963

HAL Id: hal-02382963

<https://hal.science/hal-02382963>

Submitted on 9 Nov 2020

HAL is a multi-disciplinary open access archive for the deposit and dissemination of scientific research documents, whether they are published or not. The documents may come from teaching and research institutions in France or abroad, or from public or private research centers.

L'archive ouverte pluridisciplinaire **HAL**, est destinée au dépôt et à la diffusion de documents scientifiques de niveau recherche, publiés ou non, émanant des établissements d'enseignement et de recherche français ou étrangers, des laboratoires publics ou privés.

1 **Free-standing cellulose film containing manganese**
2 **dioxide nanoparticles and its use in discoloration of**
3 **Indigo Carmine dye**

4 Larissa V. F. Oliveira^a, Simona Bennici^b, Ludovic Josien^b, Lionel Limousy^b, Marcos A.
5 Bizeto^a and Fernanda F. Camilo^{a*}

6
7 ^a *Laboratório de Materiais Híbridos, Departamento de Química, Instituto de Ciências*
8 *Ambientais, Químicas e Farmacêuticas, Universidade Federal de São Paulo – Campus*
9 *Diadema, Brazil*

10 ^b *Institut de Science des Matériaux de Mulhouse CNRS UMR 7361, Université de*
11 *Haute-Alsace, Université de Strasbourg, 3b rue Alfred Werner, 68093 Mulhouse,*
12 *Cedex, France*

13
14 * *Corresponding author: Fernanda Ferraz Camilo*

15 Laboratório de Materiais Híbridos, Instituto de Ciências Ambientais, Químicas e
16 Farmacêuticas,

17 Universidade Federal de São Paulo

18 Rua São Nicolau, 210, CEP: 09913-030, Diadema – SP, Brazil

19 Phone: +55 11 3319-3568

20 E-mail: ffcamilo@unifesp.br

21

22 **Abstract**

23 In this study, we report the production of a free-standing film of non-modified cellulose
24 impregnated with 12 wt.% of MnO₂ nanoparticles with less than 100 nm in size. The
25 method here described can be applied to the immobilization of different types of
26 nanoparticles. The film was prepared by dissolving microcrystalline cellulose in an
27 ionic liquid followed by its regeneration by adding water to the former solution. Then,
28 the wet film was impregnated with the nanoparticles by dipping it in a MnO₂ dispersion.
29 Electron microscopy images revealed manganese dioxide nanoparticles distributed not
30 only at the film surface but also in its interior. The cellulose film impregnated with
31 MnO₂ nanoparticles was capable of efficiently discolouring an Indigo Carmine dye
32 solution in 25 min upon ambient light. The film was easily removed from the dye
33 solution and repeatedly reused for at least 10 times without losing its discolouring
34 efficiency.

35

36 **Keywords:** cellulose film; manganese dioxide nanoparticles; Indigo Carmine dye;
37 discoloration tests

38 1. Introduction

39 Manganese oxide nanomaterials, due to their unique structural and chemical
40 properties, have been mainly investigated either as catalysts (D. Wang, Shin, Cheney,
41 Sposito, & Spiro, 1999)(Shaabani, Borjian Boroujeni, & Laeini, 2016) and as electrodes
42 for lithium batteries (He, Hu, Hou, & Chen, 2014)(Lee, Kim, Chen, Hammond, & Shao-
43 Horn, 2010) Owing to their combined oxidant and adsorbent capabilities, MnO₂
44 nanoparticles their combined oxidant. (Abdel Salam, 2015)(Han, Zhang, Zhao, & Feng,
45 2015)(Clarke & Johnson, 2010).However, as this nanomaterial is normally obtained in
46 the powdered form, its applicability is impaired due to the limited possibility of easy-
47 recovering from the reaction medium that prevents its reuse or adequate disposal after
48 the end of the treatment process. An alternative to overcome this problem is to support
49 the nanoparticles into suitable solid matrices.(Y. Wang et al., 2014)(Maliyekkal, Lisha,
50 & Pradeep, 2010) Cellulose, a renewable biopolymer, is an interesting material to use as
51 a film to support the nanoparticles, since it has mechanical strength, durability, and
52 water-resistance.(Zhang, Wu, Zhang, & He, 2005)(Pang, Liu, Zhang, Wu, & Sun, 2013)

53 Cellulose is the most abundant biorenewable material on earth and presents many
54 advantages of its use including low cost, biodegradability and no toxicity. However, it
55 has quite poor solubility and processability. It was just in 2002 that Rogers and co-
56 workers first dissolved cellulose with an ionic liquid (Swatloski, Spear, Holbrey, &
57 Rogers, 2002) and after it the possibility to produce cellulose films by the regeneration
58 of the dissolved cellulose with an anti-solvent was opened.(Isik, Sardon, & Mecerreyes,
59 2014) Those films could be used as support for different materials like metal or oxide
60 nanoparticles, solving the problem of nanoparticles transport and recycling in many
61 different technological applications.

62 Indigo Carmine (IC), a colorant used in food, pharmaceutical industries and mainly
63 in textile to blue jeans, becomes a serious pollutant in aquatic environments because it
64 prevents the photosynthesis of aquatic plants and algae and beyond that it may be toxic
65 to humans, causing itch, eye irritation, permanent damage to the cornea and respiratory
66 tract, if inhaled.(Othman, Mohamed, & Ibrahem, 2007)(Vautier, Guillard, & Herrmann,
67 2001) Thus, many studies have been carried out to remove this dye of wastewater.
68 Manganese dioxide nanoparticles are very effective in promoting its degradation (Vidya
69 Lekshmi, Yesodharan, & Yesodharan, 2017)(Sanchez-Botero, Herrera, & Hinestroza,
70 2017)(Mylarappa et al., 2016). However, the limited capacity of recovering these
71 nanoparticles, from the reaction medium, might be a problem.

72 Till now, only a few studies have examined the use of hybrid materials of cellulose
73 and manganese dioxide to degrade the Indigo Carmine. In 2013, (Chacón-Patiño,
74 Blanco-Tirado, Hinestroza, & Combariza, 2013) the in situ synthesis of nanostructured
75 MnO₂ onto natural fibers was reported as the catalytic activity of this material to
76 degraded the Indigo Carmine dye from water. The MnO₂-nanocomposite was able to
77 remove up to 98% of the colour present in the contaminated water samples in less than
78 5 minutes. This was one of the first report in which a biocomposite containing a
79 transition metal oxide was able to degrade an organic pollutant without the need of
80 addition of an oxygen source as oxidant such H₂O₂. In 2016, (Blanco et al., 2016) the
81 use of water hyacinth's dried matter as a support matrix for nano MnO₂ was reported as
82 well its application in the removal of Indigo Carmine dye of wastewater. The
83 degradation tests carried out in different pH indicated that the dye discoloration
84 occurred only in pH 2.3. The effectiveness of the degradation reaction in acidic pH
85 conditions is explained by the electrostatic interaction established between the negative
86 charge of the IC structure with the positive charged MnO₂ oxide surface. Since these

87 reported nanocomposites were obtained in the powdered or fiber forms, their
88 applicability in wastewater treatment could be impaired due to the limited recovering
89 capacity from the medium that prevents its reuse or adequate disposal.

90 In this sense, this paper describes a novel method to produce free-standing films of
91 non-modified cellulose impregnated with manganese dioxide nanoparticles and their
92 application in the discoloration of the indigo carmine dye upon exposure to ambient
93 light. The use of a film instead of powdered material allows a straightforward isolation
94 from treated water, avoiding the need of more complex separation methods, such as
95 centrifugation or filtration. Reports about the production of such cellulose films
96 containing MnO_2 are still scarce. In 2018, Danish and co-workers (Danish et al., 2018)
97 demonstrated the efficiency of cellulose acetate/manganese oxide thin films as
98 adsorbents for selective extraction and detection of flavone in environmental waters.
99 The use of cellulose acetate has many disadvantages since it is a synthetic cellulose and
100 has sensitivity to UV irradiation and is highly swellable in water presence, which makes its
101 use in water treatment not suitable. Recently, Peng and colleagues (Ruichao Peng,
102 Honglei Zhang, Lin Gui, Zaikun Wu & Luo, 2019) fabricated a novel porous film by
103 simply mixing mesoporous MnO_2 with porous cellulose prepared by LiOH/urea water
104 system with freeze-thaw method. The composite film was composed of MnO_2
105 microspheres spread in the reticular structure of the cellulose. The composite film was
106 used to degrade acid orange in wastewater. Compared with pure cellulose film, the
107 composite film of MnO_2 @cellulose had a better catalytic degradation efficiency, since
108 after 90 minutes the acidic orange dye degradation reached 76%.

109

110

111 2. Materials and Methods

112 2.1. Materials

113 Microcrystalline cellulose, 2-butanol (99%), potassium permanganate (99%),
114 tetramethylammonium bromide (98%) and Indigo Carmine (97%) were obtained from
115 Sigma-Aldrich and used as received without any further purifications. 1-chlorobutane
116 (99%) and 1-methylimidazole (99%) were also obtained from Sigma-Aldrich but they
117 were distilled before use.

118 2.2. Methods

119 2.2.1. Tetramethylammonium permanganate (TMAMnO₄)

120 Tetramethylammonium permanganate was prepared by using a procedure already
121 described in the literature.(Benedetti, Bazito, Ponzio, & Torresi, 2008) Succinctly, 2.54
122 g of tetramethylammonium bromide (16.5 mmol) dissolved in 10.0 mL of deionized
123 water was added dropwise in a solution of 2.37 g (15.0 mmol) of potassium
124 permanganate dissolved in 25.0 mL of deionized water. The mixture was stirred
125 vigorously for 1 hour at room temperature. The precipitate was isolated by filtration,
126 recrystallized from water and dried. The final product was a purple powder with 77%
127 yield.

128 2.2.2. Aqueous dispersion of manganese dioxide nanoparticles

129 The preparation of the aqueous dispersion of manganese dioxide nanoparticles has
130 been already described in the literature.(Benedetti et al., 2008) Briefly, 290 mg (1.50
131 mmol) of TMAMnO₄ was added in 30.0 mL of 2-butanol and 30.0 mL of deionized
132 water. The mixture was gently stirred during 1 hour, at room temperature. Then, the
133 mixture was poured into a separating funnel and the dark aqueous phase containing
134 MnO₂ was separated and used. **Water was removed from the dispersion in a rotary**

135 evaporator at 80°C and then the sample was dried in a dessicator containing silica gel.
136 This sample was denoted as MnO₂_powder.

137 **2.2.3. 1-butyl-3-methylimidazolium chloride (BMImCl)**

138 This ionic liquid was prepared by the reaction between 1-chlorobutane and 1-
139 methylimidazole following a procedure already described in the literature.(da S.
140 Oliveira et al., 2018). The BMImCl was obtained as a white solid and exhibited melting
141 point between 61-64 °C (80% yield). ¹H and ¹³C NMR were used to confirm the
142 structure.

143 **2.2.4. Cellulose solubilization and cellulose film**

144 5.00 wt% of microcrystalline cellulose (MCC) was dissolved in BMImCl at 60 °C
145 under stirring during 24 h, giving a clear and viscous solution. Then, 5.00 g of this
146 solution was spin-coated onto a glass Petri dish (15.00 cm diameter) at 500 rpm for 40
147 s. Then, water was added into the Petri dish to regenerate the cellulose as a film. The
148 membrane was washed with water until the complete removal of the residual ionic
149 liquid. The film was dried for several days in a desiccator with phosphorus pentoxide.
150 This film was denoted as cellulose film.

151 **2.2.5. Cellulose film containing manganese dioxide nanoparticles** 152 **(CEL_MnO₂NP)**

153 5.00 g of cellulose solution in BMImCl (5.00 wt%) was placed in a Petri dish (15.0
154 cm diameter). Then, the same procedure described to produce the cellulose film was
155 used, except for the drying step. After that, 30.0 mL of the aqueous dispersion of
156 manganese dioxide nanoparticles were added to that Petri dish containing the wet
157 cellulose film and they were kept in contact without stirring during 12 hours. Finally,

158 the film was washed several times with water and dried during several days at room
159 temperature, affording a dark brown cellulose film denoted as CEL_MnO₂NP.

160 **2.2.6. Indigo carmine discoloration tests**

161 The tests were carried out by placing a piece of the film CEL_MnO₂NP with 22
162 mg in 5 mL of the dye solution (20 ppm) upon ambient light (irradiation of 4 tubular
163 fluorescent light bulbs of the indoor laboratory illumination (16 W each located at
164 approximately two meters above the reaction vial)) under constant stirring. The pH of
165 the dye solution was adjusted to 2.0 with the addition of acetic acid. The discoloration
166 of the solution was monitored by electronic absorption spectroscopy at UV-Vis, by
167 accompanying the decreasing of the characteristic absorption band of Indigo Carmine at
168 610 nm. Additional tests were carried out in pH 3.0 and 4.0 using the same
169 experimental conditions.

170 **2.3. Characterizations**

171 Transmission electron microscopy images were acquired in a JEM 2100 electron
172 microscope from JEOL. The sample was prepared by depositing a drop of the MnO₂
173 dispersion onto a carbon-coated Cu microgrid.

174 Scanning electron microscopy images were acquired in a JSM-7401F microscope
175 from JEOL equipped with an energy dispersive spectrometer (EDS). The samples were
176 coated with a thin conductive layer of gold to ensure a good electrical path to ground,
177 providing improved SEM image quality.

178 Scanning transmission electron microscopy (STEM) images were registered in a
179 JSM-7900 JEOL microscope equipped with a Deben STEM detector, at an
180 accelerating voltage of 30 kV. The sample was prepared by immersing vertically a
181 piece of the cellulosic film containing the MnO₂ nanoparticles (CEL_MnO₂NP
182 sample) in a mixture of an epoxy resin and a hardener (EpoFix, Struers) for 24 hours.

183 Then, ultrathin slices were cut at with a cryogenic ultramicrotome (Leica, EM UC7).
184 These slices were left floating in water and then recovered onto TEM grids and dried
185 at room temperature before observation.

186 Particle size distribution of the MnO₂ nanoparticle dispersion was assessed by
187 using a Malvern Zetasizer Nano instrument.

188 Fourier transform infrared absorption spectra were recorded on an IR-Prestige-21
189 spectrometer from SHIMADZU, using ATR accessory (ATR-8200HA) in the range of
190 400–4000 cm⁻¹ with 4.00 cm⁻¹ of resolution.

191 Raman spectra were recorded with a RENISHAW InVia Raman spectrometer
192 working with a multichannel detection. Laser excitation was provided by a 632.8 nm
193 HeNe laser and the spectral resolution of 4.00 cm⁻¹.

194 Electronic absorption spectra were registered in an Ocean Optics
195 spectrophotometer model USB 4000 from OCEAN OPTICS. It was used quartz
196 cuvettes with 1.00 cm of optical path.

197 Nuclear magnetic resonance spectra were acquired using a VARIAN INOVA 300
198 spectrometer, operating at 300 MHz for ¹H NMR and at 75 Hz for ¹³C NMR.
199 Chloroform-D containing TMS has been used as the deuterated solvent and reference.

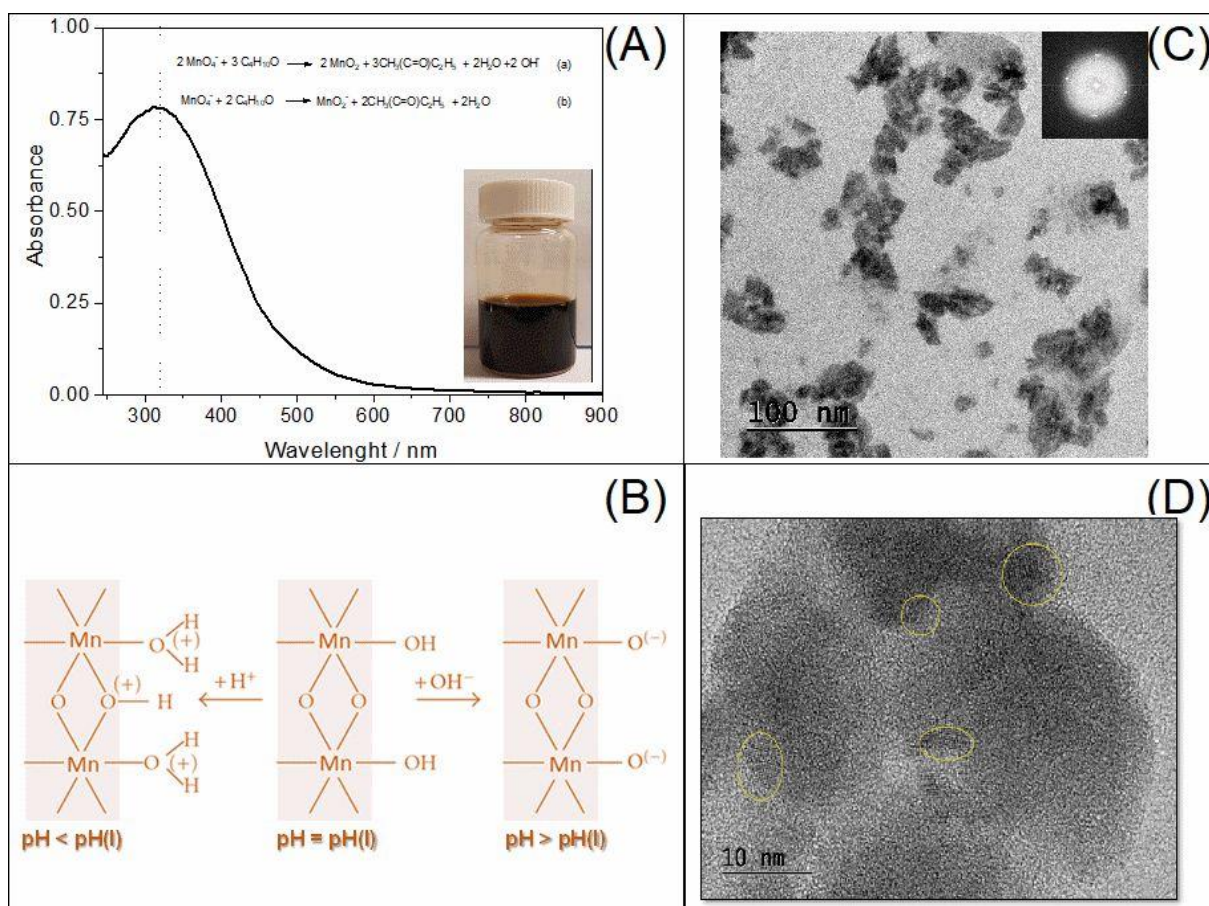
200 X-rays diffraction patterns were registered on D8-Advance diffractometer from
201 BRUKER, using Cu-K α anode (0.1542 nm), operating at 40 keV and 40 mA.

202 Thermogravimetric analysis was carried out using DTG-60 thermogravimetric
203 analyzer from SHIMADZU under airflow (100 cm³.min⁻¹) at a heating rate of 20
204 °C.min⁻¹ and the temperature range of 25 °C to 900 °C.

205 X-ray photoelectron spectroscopy (XPS) data were obtained using a THERMO
206 SCIENTIFIC K-Alpha spectrometer equipped with an aluminium monochromator Al
207 K α radiation (1486.6 eV).

208 3. Results and Discussion

209 An aqueous dispersion of manganese dioxide nanoparticles was prepared through
210 the reduction of tetramethylammonium permanganate with 2-butanol (inset in Fig. 1A),
211 which resulted in a dark brown dispersion whose electronic absorption spectrum did not
212 show bands ascribed to the presence of MnO_4^- expected at 535 nm and 545 nm,
213 indicating the complete conversion of the starting material to MnO_2 .(Fujimoto,
214 Mizukoshi, Nagata, Maeda, & Oshima, 2001) The absorption band at 320 nm was
215 attributed to a ligand-to-metal charge-transfer (LMCT) of the MnO_2 nanoparticles (Fig.
216 1A).(Brock et al., 1999a) The measured zeta potential of -50.7 ± 2.25 mV assured the
217 colloidal stability of the dispersion, since the nanoparticles were prepared in a pH higher
218 than the isoelectric point of the MnO_2 (pH_{IEP} around 4.5)(Chibowski, Grzadka, &
219 Patkowski, 2008). At this pH, the MnO_2 nanoparticles have negative charges due to the
220 ionization of terminal hydroxyl groups as schematically shown in Fig. 1B. The
221 registered TEM image (Fig. 1C) showed nanoparticles with irregular shapes and less
222 than 100 nm of size. The selected area electron diffraction (SAED) pattern (Fig 1C-right
223 top) revealed a diffuse halo without fringes with some diffraction spots, indicating that
224 the nanomaterial produced has very low crystalline domains as observed in HRTEM
225 image (Fig 1D). After the removal of water from the dispersion, the powder resultant
226 (MnO_2 _powder) was characterized by XRD, FTIR, Raman and TG (Figures 1S, 3S, 4S
227 and 5S in the supplementary information). The registered XRD pattern of the
228 MnO_2 _powder (Figure 1S in the supplementary information) corresponded to a rather
229 amorphous material, coherent with the data already published.(Benedetti et al., 2008;
230 Brock et al., 1999a)

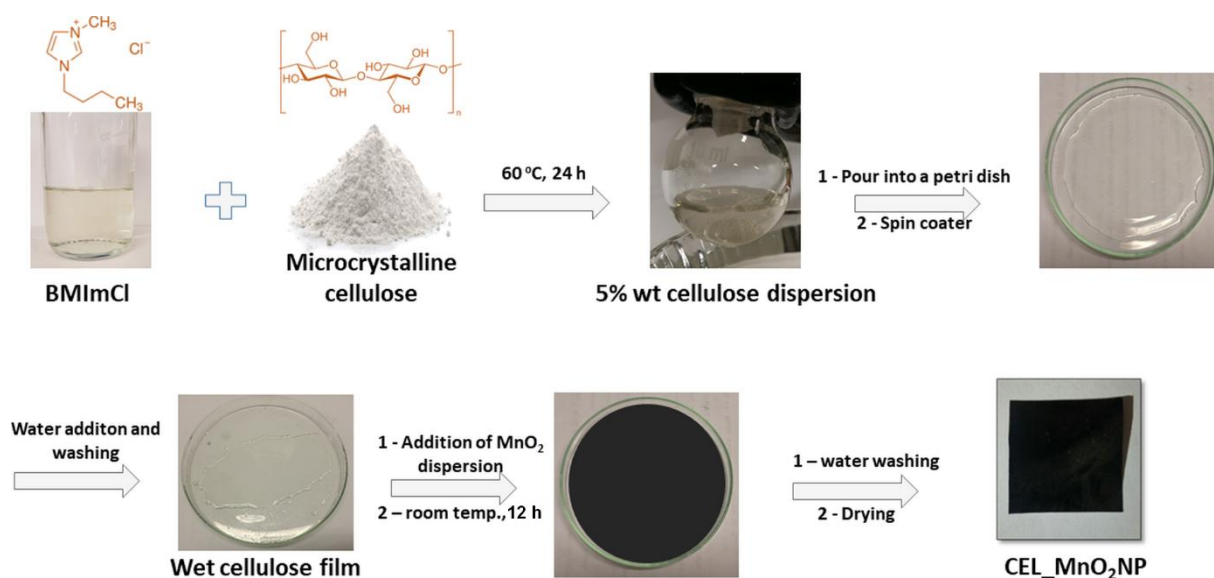


231

232 Figure 1: (A) Electronic absorption spectrum of the MnO₂ dispersion. The inset shows a photograph of
 233 the vial containing the dispersion. (B) Simplified scheme of the surface charge of MnO₂ nanoparticles
 234 according to the pH of the aqueous dispersion. (C) TEM image of the MnO₂ nanoparticles. Inset shows
 235 the registered SAED pattern. (D) HRTEM image of MnO₂ nanoparticles. The highlighted areas represent
 236 crystalline regions of the nanoparticles.

237 The preparation of the cellulose self-standing film containing MnO₂
 238 nanoparticles involved several steps as shown schematically in Figure 2. First,
 239 microcrystalline cellulose (MCC) was dissolved in the ionic liquid 1-butyl-3-
 240 methylimidazolium chloride (BMImCl) at 60 °C during 24 h. Then, the produced
 241 dispersion (5 wt% of cellulose in ionic liquid) was placed in a Petri dish, where water
 242 was added in order to promote the cellulose regeneration in the form of a film. In the
 243 next step, the aqueous dispersion of manganese dioxide nanoparticles was added to the
 244 Petri dish containing the wet cellulose film and they were kept in contact during 12
 245 hours, without stirring. **The progress of nanoparticles impregnation was monitored by**
 246 **using electronic absorption spectroscopy in the visible range. Figure 2S (supplementary**

247 information) shows the temporal evolution of the dispersion spectra profile of samples,
 248 collected every one hour, along a period of 12 h. The intensity of the band at 315 nm,
 249 ascribed to the MnO₂ nanoparticles presence, decreased with the impregnation progress.
 250 The plot of the absorbance band maxima at 315 nm as a function of impregnation time
 251 (Inset in Figure 2S) showed a straight step decrease in the first eight hours then
 252 remained practically unchanged after that. The direct regeneration of cellulose film
 253 using the MnO₂ dispersion was not possible due to the destabilization of the colloid
 254 caused by the ionic liquid presence. The impregnation in dried cellulose films was also
 255 not effective. After impregnation, the dark brown film was washed with water and
 256 dried. This film will be referred hereafter in the text as CEL_MnO₂NP.

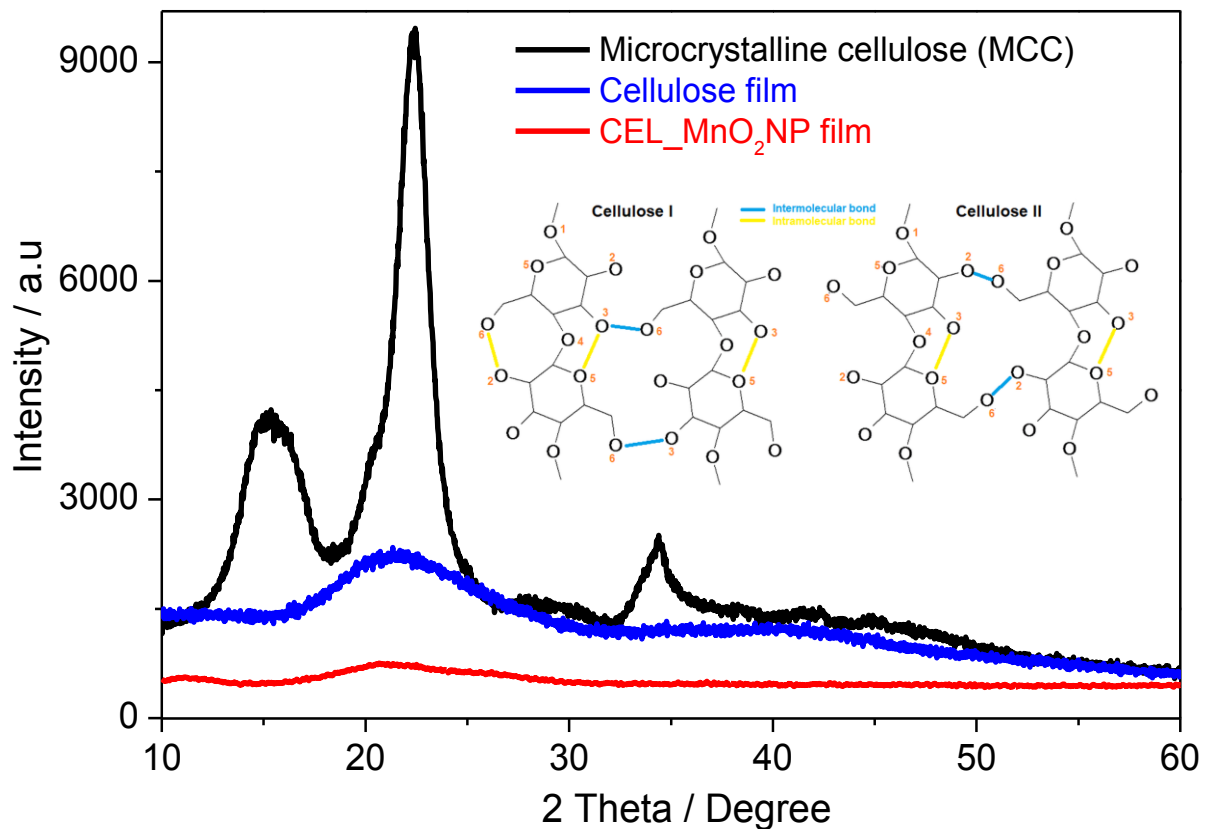


257

258 Figure 2: Scheme of the synthetic steps involved with the preparation of the CEL_MnO₂NP film.

259 Figure 3 displays a comparison between the registered XRD patterns of MCC,
 260 cellulose film and CEL_MnO₂NP film. The XRD pattern of MCC (black line – Fig. 3)
 261 shows peaks at $2\theta=15^\circ$, 22° and 34° ascribed, respectively, to the (110), (200) and
 262 (004) planes, of the type-I cellulose (Liu et al., 2011; Terinte, Ibbett, & Schuster, 2011),
 263 with around 91% of crystallinity. By regenerating the cellulose as a film (blue line – Fig

264 3), the polymer was converted to type II cellulose, that is amorphous.(Ciolacu, Ciolacu,
 265 & Popa, 2011) The presence of MnO₂ nanoparticles in the regenerated cellulose film
 266 was not detected by XRD (red line – Fig. 3), probably due to the small crystalline
 267 domains of the produced nanoparticles incorporated into the film and the high
 268 dispersion of them into the film.

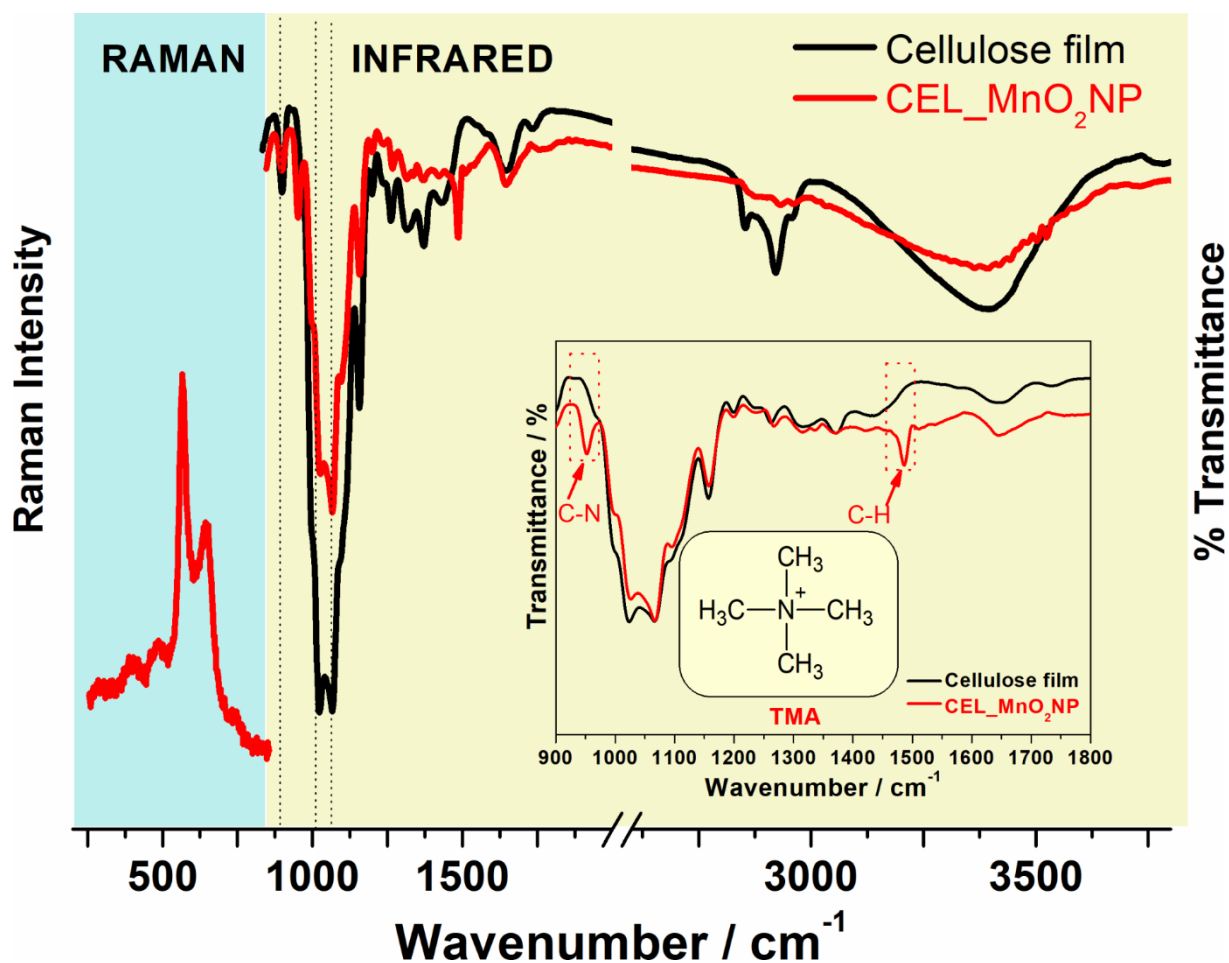


269

270 Figure 3: XRD patterns of MCC, cellulose film and CEL_MnO₂NP film. Inset shows the intermolecular
 271 and intramolecular bonds in cellulose type I and cellulose type II. The hydrogen atoms were omitted.

272 FTIR spectrum (Fig.4 – yellow rectangle) of cellulose film (black) shows a band
 273 at 901 cm⁻¹ attributed to the skeletal mode vibrations at the 1,4-β-glycosidic linkages.
 274 The C-O stretching vibrations are observed in the range between 1000 cm⁻¹ and 1100
 275 cm⁻¹. The symmetric and asymmetric C-H stretching in 2850 and 2935 cm⁻¹ and O-H
 276 axial deformation seen as a large band above 3300 cm⁻¹ are detected.(Ciolacu et al.,
 277 2011)(Liu et al., 2011) All mentioned bands were coherent with the amorphous

278 cellulose phase obtained through the dissolution of microcrystalline cellulose followed
279 by regeneration with an anti-solvent.(Ciolacu et al., 2011) In the FTIR spectrum of
280 cellulose film containing manganese dioxide nanoparticles (CEL_MnO₂NP – red line)
281 additionally to the bands of the biopolymer two bands at 1488 cm⁻¹ and 950 cm⁻¹
282 ascribed to the C-H and C-N vibrations of the tetramethylammonium cation (TMA⁺)
283 were also observed. **These two bands were also identified in the FTIR spectrum of neat**
284 **MnO₂ nanoparticles (Figure 3S)** (Bottqer & Geddes, 1965)(Harmon, Gennick, &
285 Madeira, 1974). Vibrational bands attributed to the MnO₂ were not seen in the FTIR
286 spectrum, however, in the Raman spectrum (Fig.4 – blue rectangle) the bands at 564
287 cm⁻¹ and 645 cm⁻¹ attributed to Mn-O vibrations were detected.(Xie et al.,
288 2015)(Tsubasa Uematsu, Yumi Miyamoto, Yoshiyuki Ogasawara, Kosuke Suzuki,
289 2016). **These vibrations were also observed in the Raman spectrum of neat MnO₂NP**
290 **(Figure 4S).**

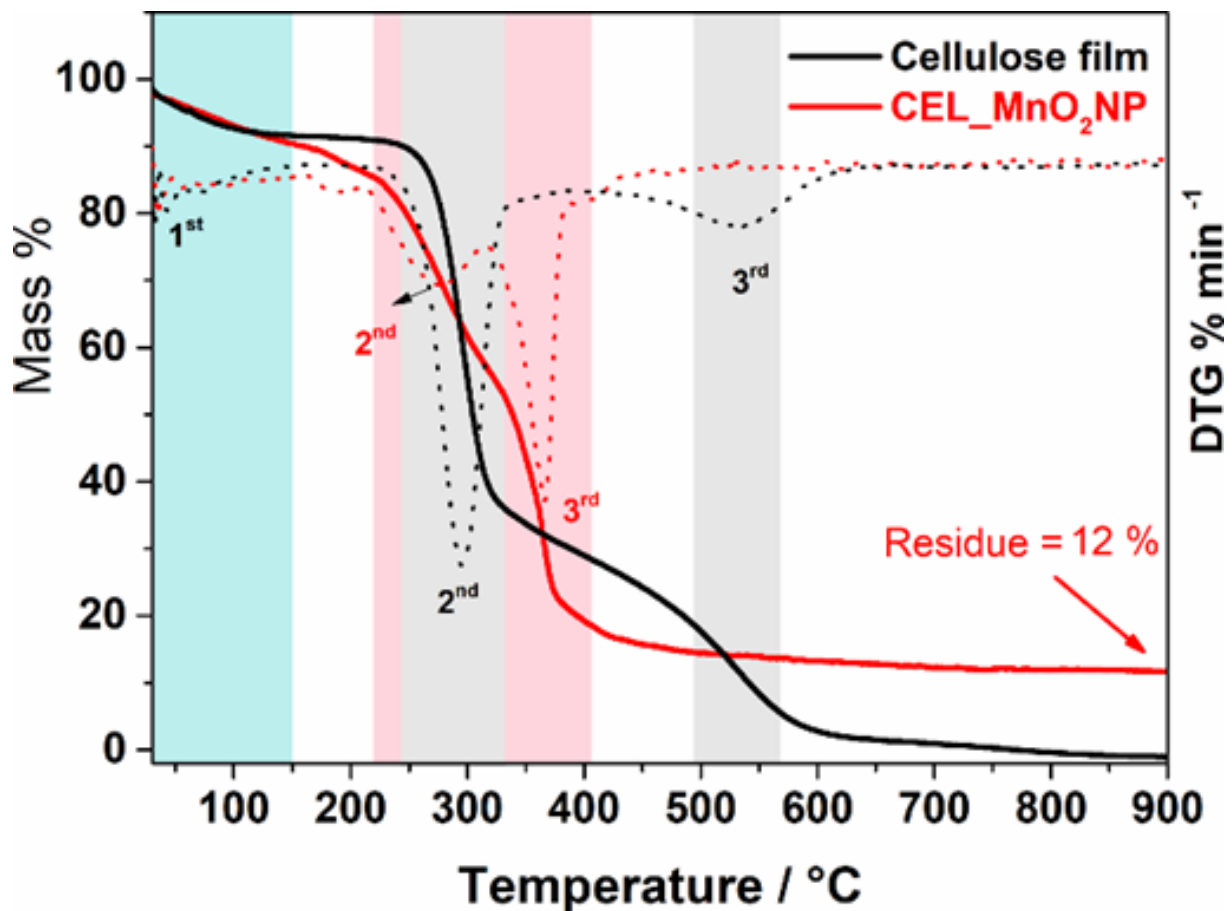


291

292 Figure 4: FTIR spectra (yellow rectangle) and Raman spectrum (blue rectangle) of cellulose and
 293 CEL_MnO₂NP films. Inset shows the enlarged region between 900 and 1800 cm⁻¹.

294 The amount of MnO₂ into the regenerated cellulose film was estimated by
 295 thermogravimetric analysis (TGA). No residue was observed in the TGA of cellulose
 296 film (black line – Fig 5), while 12 % of residue was present after the total
 297 decomposition of cellulose in the MnO₂ impregnated-film (red line – Fig 5). This
 298 residue was attributed to the amount of manganese oxide incorporated into the
 299 regenerated cellulose film. TGA and DTG curves of neat MnO₂ nanoparticle were
 300 registered (Figure 5S in supplementary information). In the TGA curve (Figure 5S) two
 301 events of thermal decomposition were observed. The first one between 30 °C and 150
 302 °C corresponding to adsorbed water molecules release and the second one between 130
 303 to 255 °C corresponding to 44 % of mass loss, which was attributed to decomposition of

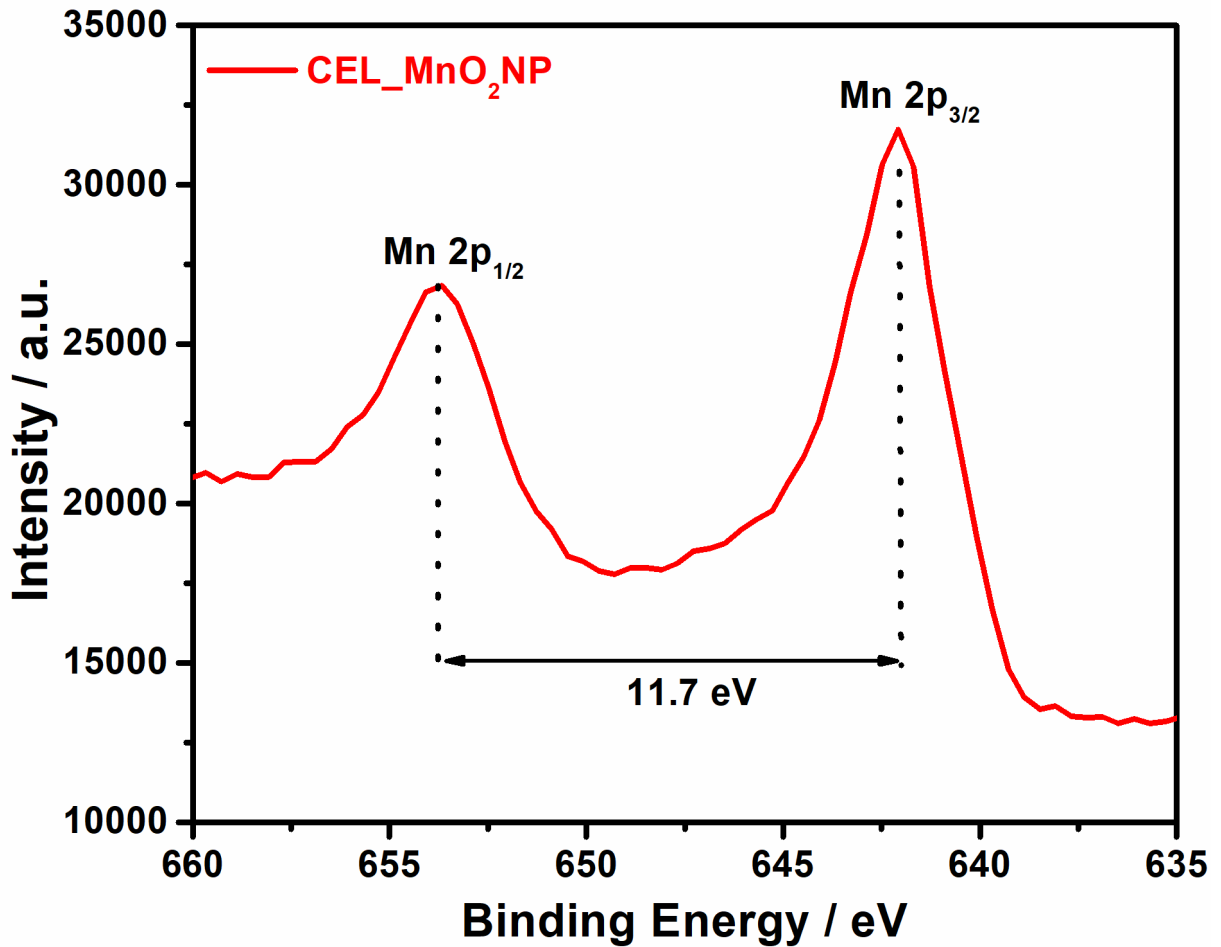
304 the TMA^+ present in the sample and also to the release of water molecules from
 305 the condensation reaction between structural hydroxyl- groups in the oxide. The residue
 306 of 36% corresponded to manganese dioxide. The first derivative of registered
 307 thermogravimetric curves of the films (Figure 5) indicated a three-step process of
 308 thermal decomposition under air atmosphere. The first one between 30 and 150 °C (blue
 309 area) corresponding to adsorbed water molecules release. The biopolymer started to
 310 decompose at 295 °C in a two-step procedure that lasted at 650 °C with no residue
 311 formation. In contrast, the cellulose film containing MnO_2 nanoparticles thermally
 312 decomposed in two consecutive events that lasted at around 490 °C with 12% of
 313 residue, indicating that nanoparticles presence promoted a decreasing in the onset
 314 temperature of decomposition of approximately 50 °C.



315

316 Figure 5: TG (solid lines) and DTG (dashed lines) curves of cellulose and $\text{CEL_MnO}_2\text{NP}$ films. The
 317 highlighted regions with coloured rectangles represent the main mass loss events.

318 The Mn 2p XPS spectrum (Figure 6) shows two peaks at 642.1 eV and 653.8 eV
319 attributed respectively to Mn 2p_{3/2} and Mn 2p_{1/2}, with spin-energy separation of 11.7 eV.
320 These peak values agree with those reported for MnO₂ indicating the predominant
321 oxidation state of +4 for the Mn present in the film.(He et al., 2014)(Y. Wang et al.,
322 2014)(Tian, Yang, Fan, & Zhang, 2011)



323

324

Figure 6: XPS spectrum of the CEL_MnO₂NP film.

325

326

327

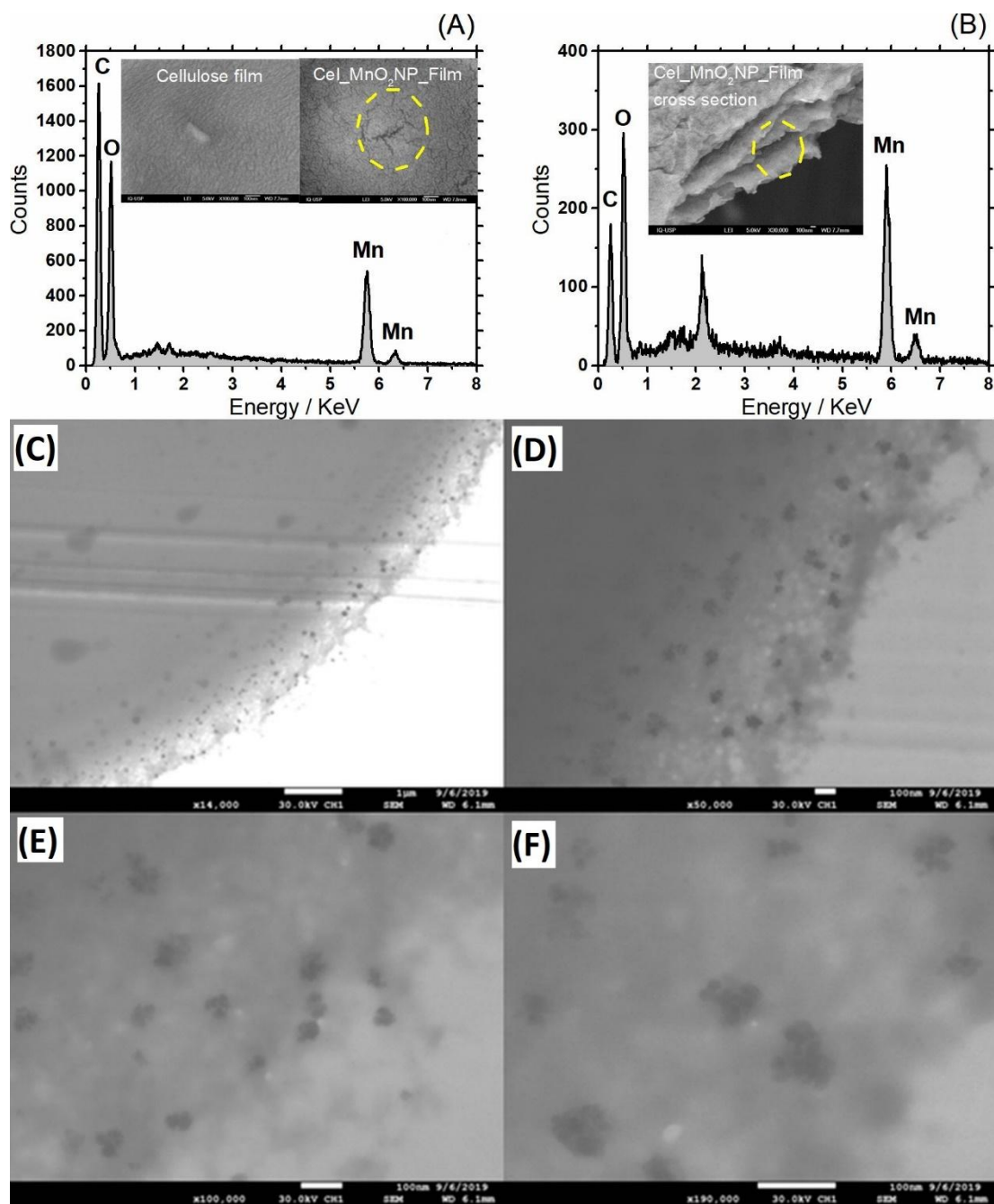
328

329

330

SEM image of the CEL_MnO₂NP film (Fig.7A inset) exhibited typical features of regenerated cellulose films with a smooth and uniform surface. These characteristics are probably due to the destruction of the cellulose crystalline structure, however, the fiber contours were observed in the regenerated films due to the maintaining of the strong hydrogen bonding of cellulose during film-forming (Zhang et al., 2005) MnO₂ particles were not observed due to their small size with low electronic contrast.

331 However, the elemental analysis using EDS (Fig.7A) reveals the presence of manganese
332 at the surface due to signals at 5.8 and 6.4 keV besides the oxygen and carbon peaks,
333 which are present in the grid and cellulose. SEM image of a fractured cross-section of
334 the film shows a layered structure composed of hydrogen bond networks among
335 cellulose chains (Fig. 7B inset). MnO₂ particles were not seen but the elemental analysis
336 (Fig. 7B) confirmed their presence inside in the film and not only in the surface. **STEM**
337 **images of the CEL_MnO₂NP film were obtained on the sample prepared with a specific**
338 **procedure described in the experimental part. Fig.7C shows that the MnO₂ particles are**
339 **dispersed homogeneously in the cellulosic film all along the thickness. At higher**
340 **enlargements (Fig 7D and E) it is possible to observe that these particles consist in the**
341 **agglomeration of smaller MnO₂ nanoparticles, some of them being isolated. In Fig 7F,**
342 **the size of the small nanoparticles can be evaluated to be close to 10 nm. The particle**
343 **size distribution of the MnO₂ suspension was performed by Dynamic Light Scattering in**
344 **order to evaluate the size of the nanoparticles. Results show that the suspension presents**
345 **a bimodal dispersion with particle average sizes corresponding to 8 and 79 nm,**
346 **respectively. This datum confirms the STEM observations and the presence of both**
347 **single and agglomerated MnO₂ nanoparticles in the cellulosic film.**

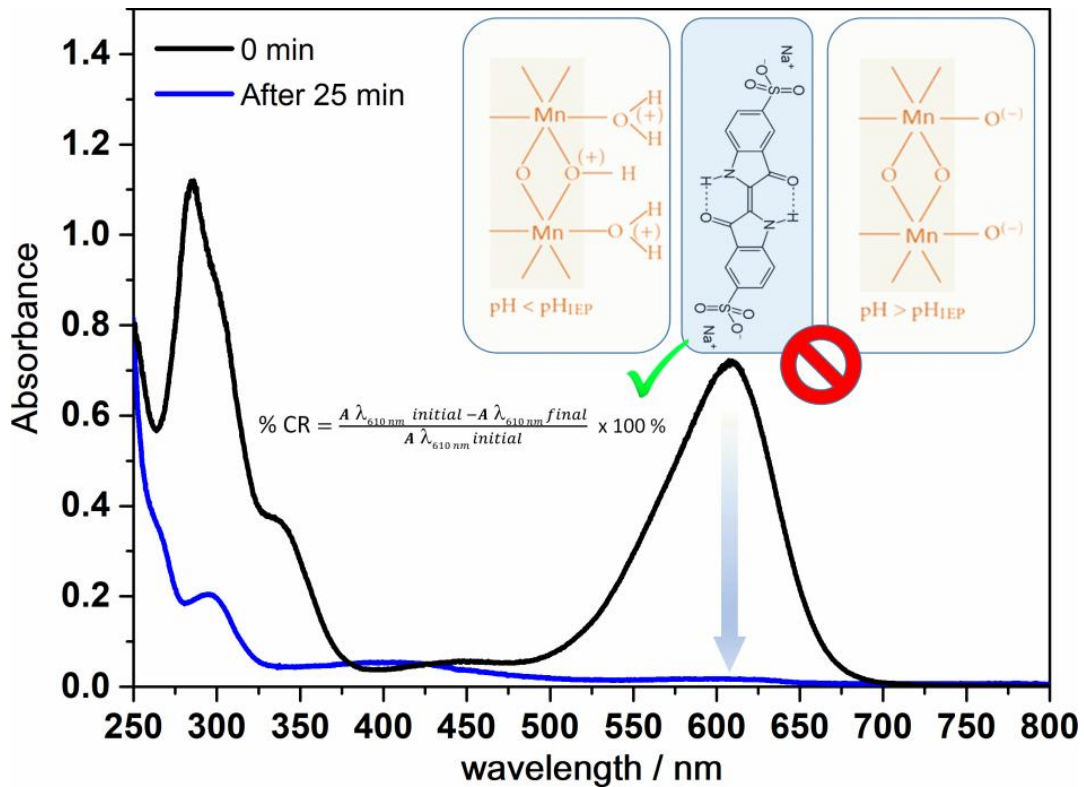


348

349 Figure 7: SEM images and EDS analysis of the region circled in yellow of the top surface (A) and cross
 350 section (B) of the CEL_MnO₂NP film (C-F) STEM images of the CEL_MnO₂NP film at different
 351 magnification ((a) x14 000, (b) x50 000, (c) x100 000 and (d) x190 000). *peak at 2.1 KeV is from the
 352 thin layer of gold used to coat the sample.

353 The indigo carmine discoloration test was carried out by placing 22 mg of a
 354 piece of the film CEL_MnO₂NP in contact with 5 mL of the dye solution (20 ppm)
 355 under ambient light exposure and constant stirring. It is worth to mention that this film
 356 had about 2.6 mg of impregnated MnO₂ nanoparticles content. The pH of the dye

357 solution was maintained at 2 by the addition of acetic acid. The discoloration was
 358 monitored by UV-Vis spectroscopy, by accompanying the decreasing of the
 359 characteristic absorption band of Indigo Carmine at 610 nm (Fig.8).



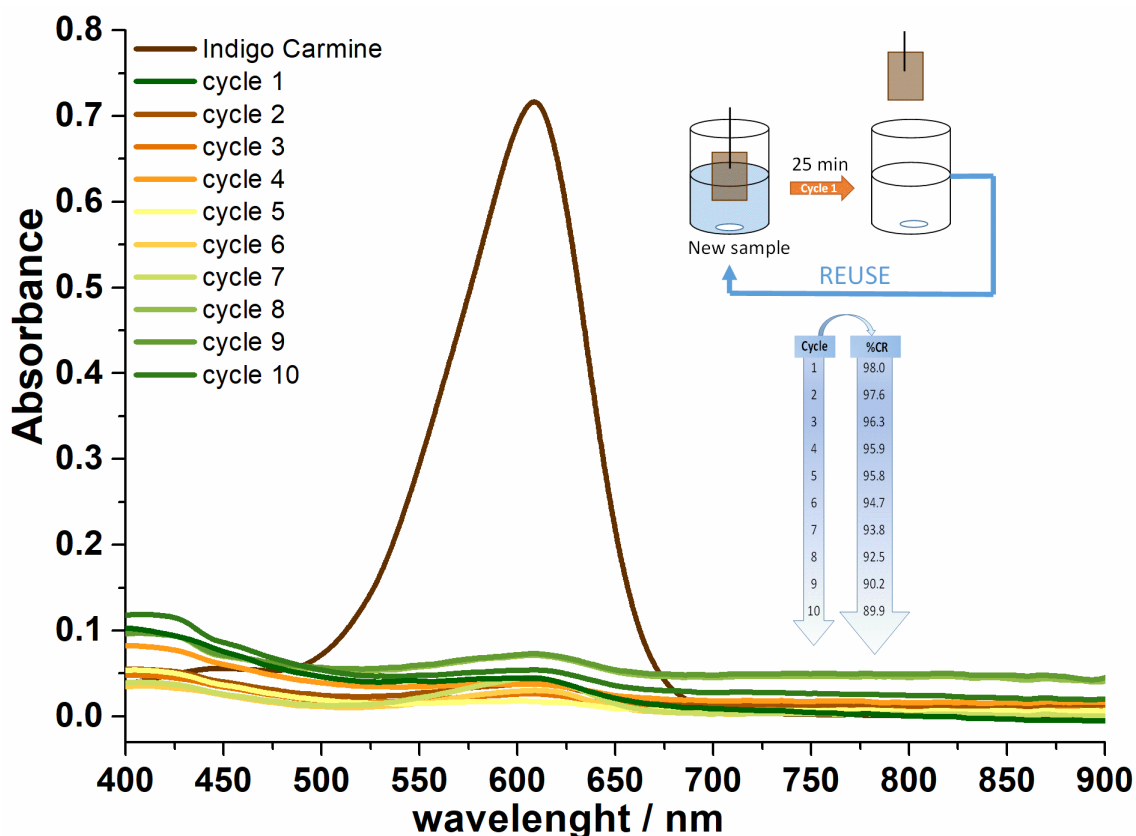
360

361 Figure 8: Absorbance decay of indigo carmine dye in water (20 ppm). Inset: Interactions between Indigo
 362 Carmine and MnO₂ in different pH and % CR equation.

363 The color removal (% CR) was estimated by the percentage ratio between the
 364 absorbance at 610 nm before and after contact with the film, which equation was shown
 365 in the inset in Figure 8. % CR values higher than 90 % were considered as complete
 366 discoloration. After 25 minutes, complete color removal was observed. In neutral
 367 conditions, the tests were unsuccessful even after hours, due to the ineffective
 368 interaction of the manganese dioxide contained in the film and the dye molecules. As
 369 stated by (Chacón-Patiño et al., 2013) at pH lower than the isoelectric point of the
 370 manganese dioxide (pH_{IEP}= 4.5), the positive surface of the nanoparticles (Mn–OH₂⁺
 371 groups) has favorable electrostatic interactions with the dye bearing a negative (anionic)

372 charge. At neutral conditions, there is a repulsive electrostatic force, since both species
373 are negatively charged (inset in Fig.8). We also evaluated the influence of pH value on
374 the discoloration time of indigo carmine at pH=3.0 and 4.0. The complete colour
375 removal (%CR higher than 90 %) were achieved after 60 and 180 minutes, respectively,
376 showing the importance of the MnO₂ oxide surface charge on the discoloration
377 behaviour of indigo carmine. Control tests were made under the same conditions,
378 without the film or using a cellulose film, but no discoloration was observed, even after
379 a long time (24 h). The mechanistic degradation of indigo carmine by the identification
380 of the intermediary compounds produced during the degradation has already been
381 studied in the literature by mass spectrometry(Chacón-Patiño et al., 2013; Zaied et al.,
382 2011).

383 In addition, it was possible to reuse the film for at least 10 cycles observing only
384 a decrease of 10% in the % CR from the first to last cycle (Fig.9).



385

386 Figure 9: Absorbance decay of indigo carmine dye in water (20 ppm) after 25 min for different reuse
 387 cycles Inset: % CR values for 10 reuses.

388

389 4. Conclusions

390 A free-standing non-modified cellulose film containing manganese dioxide
 391 nanoparticles was easily prepared. The film contains about 12 wt.% of manganese
 392 dioxide. This method can be used to immobilize other types of nanoparticles. The
 393 cellulose film containing manganese dioxide nanoparticles was capable of discoloring
 394 an Indigo Carmine solution efficiently under ambient light with no need of
 395 centrifugation and filtration steps to remove it from the dye solution. It could be reused
 396 at least 10 times with almost the same efficiency.

397

398

399 Acknowledgments

400 This study was financed in part by the Coordenação de Aperfeiçoamento de Pessoal
401 de Nível Superior – Brasil (CAPES) – Finance Code 001. The authors gratefully
402 acknowledge the financial support from FAPESP (grant number 2018/20826-4),
403 professor Vera Constantino (IQ-USP) for provided the use of the DLS/Zeta potential
404 equipment and Brazilian Nanotechnology National Laboratory (LNNano) for the XPS
405 experiments (project number XPS - 24897).

406 References

- 407 Abdel Salam, M. (2015). Synthesis and characterization of novel manganese oxide nanocorals
408 and their application for the removal of methylene blue from aqueous solution. *Chemical*
409 *Engineering Journal*, 270, 50–57. <https://doi.org/10.1016/j.cej.2015.02.022>
- 410 Benedetti, T., Bazito, F. F. C., Ponzio, E. A., & Torresi, R. M. (2008). Electrostatic Layer-by-
411 Layer Deposition and Electrochemical Characterization of Thin Films Composed of MnO
412 2 Nanoparticles in a Room-Temperature Ionic Liquid. *Langmuir*, 24(29), 3602–3610.
413 <https://doi.org/10.1021/la702347x>
- 414 Blanco, C., César, A., Hugo, R., Cuervo Blanco, T., Sierra Ávila, C. A., & Zea Ramírez, H. R.
415 (2016). Nanostructured MnO₂ catalyst in *E. crassipes* (water hyacinth) for indigo carmine
416 degradation. *Revista Colombiana de Química*, 45(2), 30–38.
417 <https://doi.org/10.15446/rev.colomb.quim.v45n2.60395>
- 418 Bottger, G. L., & Geddes, A. L. (1965). The infrared spectra of the crystalline
419 tetramethylammonium halides. *Spectrochimica Acta*, 21(10), 1701–1708.
420 [https://doi.org/10.1016/0371-1951\(65\)80082-0](https://doi.org/10.1016/0371-1951(65)80082-0)
- 421 Brock, S. L., Sanabria, M., Suib, S. L., Urban, V., Thiyagarajan, P., & Potter, D. I. (1999a).
422 Particle Size Control and Self-Assembly Processes in Novel Colloids of Nanocrystalline
423 Manganese Oxide. *The Journal of Physical Chemistry B*, 103(35), 7416–7428.
424 <https://doi.org/10.1021/jp991009u>
- 425 Brock, S. L., Sanabria, M., Suib, S. L., Urban, V., Thiyagarajan, P., & Potter, D. I. (1999b).
426 Particle Size Control and Self-Assembly Processes in Novel Colloids of Nanocrystalline
427 Manganese Oxide. *The Journal of Physical Chemistry B*, 103(35), 7416–7428.

- 428 <https://doi.org/10.1021/jp991009u>
- 429 Chacón-Patiño, M. L., Blanco-Tirado, C., Hinestroza, J. P., & Combariza, M. Y. (2013).
430 Biocomposite of nanostructured MnO₂ and fique fibers for efficient dye degradation.
431 *Green Chemistry*, 15(10), 2920–2928. <https://doi.org/10.1039/c3gc40911b>
- 432 Chibowski, S., Grzadka, E., & Patkowski, J. (2008). Comparison of the influence of a kind of
433 electrolyte and its ionic strength on the adsorption and electrokinetic properties of the
434 interface: Polyacrylic acid/MnO₂/electrolyte solution. *Colloids and Surfaces A:
435 Physicochemical and Engineering Aspects*, 326(3), 191–203.
436 <https://doi.org/10.1016/j.colsurfa.2008.05.038>
- 437 Ciolacu, D., Ciolacu, F., & Popa, V. I. (2011). Amorphous Cellulose – Structure and
438 Characterization. *Cellulose Chemistry and Technology*, 45(1–2), 13–21.
439 <https://doi.org/10.1163/156856198X00740>
- 440 Clarke, C. E., & Johnson, K. L. (2010). Oxidative breakdown of acid orange 7 by a manganese
441 oxide containing mine waste: Insight into sorption, kinetics and reaction dynamics.
442 *Applied Catalysis B: Environmental*, 101(1–2), 13–20.
443 <https://doi.org/10.1016/j.apcatb.2010.08.020>
- 444 Danish, E. Y., Marwani, H. M., Alhazmi, M. A., Khan, S. B., Bakhsh, E. M., & Asiri, A. M.
445 (2018). Assessment of cellulose acetate / manganese oxide thin film as adsorbent for
446 selective extraction of flavone. *Bull. Mater. Sci.*, 41, 47–54.
447 <https://doi.org/10.1007/s12034-018-1569-3>
- 448 Fujimoto, T., Mizukoshi, Y., Nagata, Y., Maeda, Y., & Oshima, R. (2001). Sonolytical
449 preparation of various types of metal nanoparticles in aqueous solution. *Scripta
450 Materialia*, 44(8–9), 2183–2186. [https://doi.org/10.1016/S1359-6462\(01\)00900-9](https://doi.org/10.1016/S1359-6462(01)00900-9)
- 451 Han, B., Zhang, M., Zhao, D., & Feng, Y. (2015). Degradation of aqueous and soil-sorbed
452 estradiol using a new class of stabilized manganese oxide nanoparticles. *Water Research*,
453 70, 288–299. <https://doi.org/10.1016/j.watres.2014.12.017>
- 454 Harmon, K. M., Gennick, I., & Madeira, S. L. (1974). Hydrogen bonding. IV. Correlation of
455 infrared spectral properties with C-H···X hydrogen bonding and crystal habit in
456 tetramethylammonium ion salts. *Journal of Physical Chemistry*, 78(25), 2585–2591.
457 <https://doi.org/10.1021/j100618a012>
- 458 He, S., Hu, C., Hou, H., & Chen, W. (2014). Ultrathin MnO₂ nanosheets supported on cellulose
459 based carbon papers for high-power supercapacitors. *Journal of Power Sources*, 246, 754–

- 460 761. <https://doi.org/10.1016/j.jpowsour.2013.08.038>
- 461 Isik, M., Sardon, H., & Mecerreyes, D. (2014). Ionic liquids and cellulose: Dissolution,
462 chemical modification and preparation of new cellulosic materials. *International Journal*
463 *of Molecular Sciences*, 15(7), 11922–11940. <https://doi.org/10.3390/ijms150711922>
- 464 Lee, S. W., Kim, J., Chen, S., Hammond, P. T., & Shao-Horn, Y. (2010). Carbon
465 Nanotube/Manganese Oxide Ultrathin Film Electrodes for Electrochemical Capacitors.
466 *ACS Nano*, 4(7), 3889–3896. <https://doi.org/10.1021/nn100681d>
- 467 Liu, Z., Wang, H., Li, Z., Lu, X., Zhang, X., Zhang, S., & Zhou, K. (2011). Characterization of
468 the regenerated cellulose films in ionic liquids and rheological properties of the solutions.
469 *Materials Chemistry and Physics*, 128(1–2), 220–227.
470 <https://doi.org/10.1016/j.matchemphys.2011.02.062>
- 471 Maliyekkal, S. M., Lisha, K. P., & Pradeep, T. (2010). A novel cellulose – manganese oxide
472 hybrid material by in situ soft chemical synthesis and its application for the removal of Pb
473 (II) from water. *Journal of Hazardous Materials*, 181(1–3), 986–995.
474 <https://doi.org/10.1016/j.jhazmat.2010.05.112>
- 475 Mylarappa, M., Lakshmi, V. V., Mahesh, K. R. V., Nagaswarupa, H. P., Prashantha, S. C.,
476 Siddeswara, D. M. K., & Raghavendra, N. (2016). Electro chemical and photo catalytic
477 studies of MnO₂ nanoparticle from waste dry cell batteries. *Nanosystems: Physics,*
478 *Chemistry, Mathematics*, 7(4), 657–661. [https://doi.org/10.17586/2220-8054-2016-7-4-](https://doi.org/10.17586/2220-8054-2016-7-4-657-661)
479 [657-661](https://doi.org/10.17586/2220-8054-2016-7-4-657-661)
- 480 Othman, I., Mohamed, R. M., & Ibrahim, F. M. (2007). Study of photocatalytic oxidation of
481 indigo carmine dye on Mn-supported TiO₂. *Journal of Photochemistry and Photobiology*
482 *A: Chemistry*, 189(1), 80–85. <https://doi.org/10.1016/j.jphotochem.2007.01.010>
- 483 Pang, J., Liu, X., Zhang, X., Wu, Y., & Sun, R. (2013). Fabrication of cellulose film with
484 enhanced mechanical properties in ionic liquid 1-allyl-3-methylimidazolium chloride
485 (AmimCl). *Materials*, 6(4), 1270–1284. <https://doi.org/10.3390/ma6041270>
- 486 Roselaine, A., Oliveira, S., Bizeto, M. A., da Silva Oliveira, R., Bizeto, M. A., Camilo, F. F., ...
487 Camilo, F. F. (2018). Production of self-supported conductive films based on cellulose,
488 polyaniline and silver nanoparticles. *Carbohydrate Polymers*, 199(6), 84–91.
489 <https://doi.org/10.1016/j.carbpol.2018.06.049>
- 490 Ruichao Peng, Honglei Zhang, Lin Gui, Zaikun Wu, P. Y., & Luo, and Y. (2019). Facile
491 Synthesis of MnO₂@ Cellulose Composite Film. *Environmental Engineering Science*,

492 36(5), 1–6. <https://doi.org/10.1089/ees.2018.0442>

493 Sanchez-Botero, L., Herrera, A., & Hinestroza, J. (2017). Oriented Growth of α -MnO₂
494 Nanorods Using Natural Extracts from Grape Stems and Apple Peels. *Nanomaterials*,
495 7(6), 117–132. <https://doi.org/10.3390/nano7050117>

496 Shaabani, A., Borjian Boroujeni, M., & Laeini, M. S. (2016). Porous chitosan-MnO₂
497 nanohybrid: a green and biodegradable heterogeneous catalyst for aerobic oxidation of
498 alkylarenes and alcohols. *Applied Organometallic Chemistry*, 30(3), 154–159.
499 <https://doi.org/10.1002/aoc.3412>

500 Swatloski, R. P., Spear, S. K., Holbrey, J. D., & Rogers, R. D. (2002). Dissolution of Cellulose
501 with Ionic Liquids. *Journal of the American Chemical Society*, 124(18), 4974–4975.
502 <https://doi.org/10.1021/ja025790m>

503 Terinte, N., Ibbett, R., & Schuster, K. C. (2011). OVERVIEW ON NATIVE CELLULOSE
504 AND MICROCRYSTALLINE CELLULOSE I STRUCTURE STUDIED BY X-RAY
505 DIFFRACTION (WAXD): COMPARISON BETWEEN MEASUREMENT
506 TECHNIQUES. *Lenzinger Berichte*, 89, 118–131.

507 Tian, W., Yang, H., Fan, X., & Zhang, X. (2011). Catalytic reduction of NO_x with NH₃ over
508 different-shaped MnO₂ at low temperature. *Journal of Hazardous Materials*, 188(1–3),
509 105–109. <https://doi.org/10.1016/j.jhazmat.2011.01.078>

510 Tsubasa Uematsu, Yumi Miyamoto, Yoshiyuki Ogasawara, Kosuke Suzuki, K. Y. and N. M.
511 (2016). Molybdenum-doped α -MnO₂ as an efficient reusable heterogeneous catalyst for
512 aerobic sulfide oxygenation. *Catalysis Science & Technology*, 6, 222–233.
513 <https://doi.org/10.1039/C5CY01552A>

514 Vautier, M., Guillard, C., & Herrmann, J.-M. (2001). Photocatalytic Degradation of Dyes in
515 Water: Case Study of Indigo and of Indigo Carmine. *Journal of Catalysis*, 201(1), 46–59.
516 <https://doi.org/10.1006/jcat.2001.3232>

517 Vidya Lekshmi, K. P., Yesodharan, S., & Yesodharan, E. P. (2017). MnO₂ and MnO₂/TiO₂
518 mediated, persulphate enhanced photocatalysis for the removal of indigo carmine dye
519 pollutant from water. *European Chemical Bulletin*, 6(5), 177–191.
520 <https://doi.org/10.17628/ecb.2017.6.177-191>

521 Wang, D., Shin, J. Y., Cheney, M. A., Sposito, G., & Spiro, T. G. (1999). Manganese dioxide as
522 a catalyst for oxygen-independent atrazine dealkylation. *Environmental Science and*
523 *Technology*, 33(18), 3160–3165. <https://doi.org/10.1021/es990419t>

524 Wang, Y., Zhang, X. X., He, X., Zhang, W., Zhang, X. X., & Lu, C. (2014). In situ synthesis of
525 MnO₂ coated cellulose nanofibers hybrid for effective removal of methylene blue.
526 *Carbohydrate Polymers*, *110*, 302–308. <https://doi.org/10.1016/j.carbpol.2014.04.008>

527 Xie, Y., Yu, Y., Gong, X., Guo, Y., Guo, Y., Wang, Y., & Lu, G. (2015). Effect of the crystal
528 plane figure on the catalytic performance of MnO₂ for the total oxidation of propane.
529 *CrystEngComm*, *17*, 3005–3014. <https://doi.org/10.1039/C5CE00058K>

530 Zaied, M., Chutet, E., Peulon, S., Bellakhal, N., Desmazières, B., Dachraoui, M., & Chaussé, A.
531 (2011). Environmental Spontaneous oxidative degradation of indigo carmine by thin films
532 of birnessite electrodeposited onto SnO₂. *Applied Catalysis B, Environmental*, *107*(1–2),
533 42–51. <https://doi.org/10.1016/j.apcatb.2011.06.035>

534 Zhang, H., Wu, J., Zhang, J., & He, J. (2005). 1-allyl-3-methylimidazolium chloride room
535 temperature ionic liquid: A new and powerful nonderivatizing solvent for cellulose.
536 *Macromolecules*, *38*(20), 8272–8277. <https://doi.org/10.1021/ma0505676>

537

538

539

540

541